Hindawi
Advances in Civil Engineering
Volume 2021, Article ID 6610534, 11 pages
https://doi.org/10.1155/2021/6610534

Research Article

Experimental-Numerical Study of Indexation of Scenic Road Vertical Alignment in China

Ronghua Wang,[1] **Xingliang Liu**,[2] **and Zhe Yuan**[3]

[1]*College of Architecture and Civil Engineering, Beijing University of Technology, Beijing 100124, China*
[2]*College of Traffic & Transportation, Chongqing Jiaotong University, Chongqing 400074, China*
[3]*Jinan Urban and Rural Transportation Bureau, Jinan 250014, China*

Correspondence should be addressed to Xingliang Liu; xingliang1125@outlook.com

Received 19 October 2020; Accepted 3 March 2021; Published 22 March 2021

Academic Editor: Zhanping You

The vertical alignment design method of road in scenic spots does not evolve enough along the vehicle's rapid variation. Values of the maximum longitudinal slope (MLS) and longest slope length (LSL) applicable to scenic roads used by the environmental-friendly vehicle (EFV) are not provided. To compensate for this shortage, a multibody vehicle dynamic model in uphill traving is built, providing the static equilibrium state and dynamic balancing process of a typical vehicle. MLS and LSL values in scenic roads are obtained based on this model through numerical simulation, considering typical EFV, maximum velocity loss (MVL), and ideal velocity loss (IVL). Field experiments for verifying the results are also carried out in Huashan Mountain, Cuihua Mountain National Park, and Taiping Forest Park, using two EFV types. MLS and LSL values in scenic roads applicable to EFV obtained in this research vary from 7.8% to 10.2% and 200 to 955 m, respectively, and both are larger than the corresponding values in current criteria. According to verification results, relative errors of climbing velocity vary from 0.0104 to 0.0205, showing the dynamic model's accuracy and further proving the practicality of MLS and LSL values obtained. The results obtained in this research lay a foundation for establishing the scenic-road vertical alignment design method.

1. Introduction

In early 1900s, the first steam-powered carriage entered Yosemite National Park in U.S. Since then, automobiles have become the major method adopted by travelers to experience landscape resources in scenic spots. The reasonable and environmental-friendly roadway alignment design would promote this experience. The vertical alignment design is an essential part of the roadway alignment design. And, the vehicle's dynamic performance determines the technical index values of vertical alignment. The scenic road vertical alignment design method largely relies on contemporary typical vehicle's dynamic characters [1]. However, an environmentally friendly vehicle (EFV) with electric- or ethanol-powered engine has been introduced in scenic spots in China in recent years, and private vehicles cannot enter in the scenic spot for environment protection. The dynamic performance of EFV is lower than that of the oil-powered vehicle for the lower power of EFV, which would influence the maximum longitudinal gradient and the length of the longitudinal slope. On account of smaller pollutant emissions from EFV compared with oil-powered vehicles during the driving of EFV in the scenic spot, it can be beneficial for the sustainable development for scenic spot management. Therefore, providing a scenic road vertical alignment design method applicable to EFV is important and promising.

In past several decades, series studies related to scenic road or scenic spot traffic have been conducted, which concentrated on recreational routes' choices [2], tourism forecasting [3, 4], emissions and noise [4, 5], wilderness retaining [6, 7], alignment design [8, 9], etc., using both field research and simulation. However, the vertical alignment design method of roads in scenic spots did not evolve enough with vehicle's rapid variation. There are still lack of the

maximum longitudinal slope (MLS) value and longest slope length (LSL) value applicable to scenic roads used by EFV.

In order to compensate abovementioned shortages and promote the scenic road design method, this study focuses on vertical alignment based on the EFV dynamic character, providing some basis to scenic road design practices. Indices of MLS and LSL in scenic road representing vertical alignment are chosen as objectives in this study. Scenic spots and typical vehicle types selected in this research are selected in China, and the results obtained are also expected to be used in domestic conditions Indicators of MLS and LSL used in ordinary rural roads in current China design criteria are shown in Table 1 [10, 11].

Data from Table 1 are obtained based on the typical heavy vehicle on current ordinary rural roads in China. However, EFV used on scenic road reflects different dynamic characters. It is necessary to reconsider these indicators based on typical EFV. Moreover, indicators used in current scenic roads are usually directly chosen from the grey area in Table 1. But in practice, the longitudinal slope in scenic roads is sometimes larger than 10%, exceeding the boundary of current criteria. In that, to obtain appropriate MLS and LSL in scenic roads used by EFV, a dynamic model of the multibody vehicle considering the complex and real uphill travel environment is built. Based on this model, MLS and LSL in scenic roads are calculated using numerical simulation incorporating typical EFV determined by field studies. In addition, to prove the practicality of calculated MLS and LSL, field experiments are carried out to verify the multibody vehicle model.

Table 1: MLS and LSL used in current rural road design criteria in China.

Operation velocity (km/h)	120	100	80	60	40	30	20
MLS (%)	3	4	5	6	7	8	9
Longitudinal slope (%)	LSL (m)						
3	900	100	1100	1200	—	—	—
4	700	800	900	1000	1100	1100	1200
5	—	600	700	800	900	900	1000
6	—	—	500	600	700	700	800
7	—	—	—	—	500	500	600
8	—	—	—	—	300	300	400
9	—	—	—	—	—	200	300
10	—	—	—	—	—	—	200

2. Literature Review

The related works of scenic road or scenic spot traffic could be divided into four aspects, which are travel traffic analysis, ecological road construction method, tourism transport economy problems, and scenic road geometric design. In travel traffic analysis, approaches focused on tourists or recreational travelers' routes choices draw some attention [2, 12]. Further, empirical and simulated data were analyzed using quantitative and qualitative methods to forecast tourists [3, 5], and models focusing on traffic capacity of roads in scenic spots and protected lands were also investigated [13, 14]. In the second aspect of the ecological road construction method, it was stated that, with an extension of the scenic road network and increase of travel traffic volume, harmful effects including traffic accidents, emissions, and noise will be imposed on local residents, flora, and fauna [4, 7, 15, 16]. Therefore, public concerns on scenic road construction and maintaining have existed for several decades, by claiming a retaining of road-less wilderness [6, 17]. The third aspect of tourism transport economy problems mainly derived from explosive growth of visitors' popularity. This is a problem governed by management departments of scenic spots [18, 19], and their objective is to gain a balance between scenic road charge and travelers' acceptance. Therefore, road toll strategies and travelers' demand models were widely studied [9, 20, 21].

In the fourth aspect of the scenic road geometric design method, which is also the subject of this paper, the most important and classical works are "The Highway Capacity Manual (HCM)" [22] and "A Policy on Geometric Design of Highways and Streets" [8]. These two guidelines provided the principle of the road alignment design, which was as "grades or straight vertical segments are designed to be steep enough to allow for longitudinal drainage, but not so steep as to pose a danger to vehicles through inadvertent excessive speed at downhill segments (and, conversely, difficulty of climbing steep uphill segments that pose safety risks where there are inadequate passing opportunities)." Unfortunately, there is little standard or guideline to guide the geometric design of roads in the scenic spot in China. The most frequently used method of designing the alignment of scenic roads is under the Technical Standard of Highway Engineering [23] and Design Specification for Highway Alignment [10]. The designing method in these materials must give the consideration of multiple vehicle types, such as medium-sized vehicles with loading capacity between 7 tons and 20 tons, or large vehicles with loading capacity over 20 tons. These types of vehicles are forbidden to entering in the scenic spot.

Following this principle, many related studies have been carried out. Some studies paid their attentions on methods of ensuring consistent roadway alignment to meet the drivers' demand [24, 25]. Some studies focused on the sight distance constrained by vertical curvature, which consequently determined the operating speed [26]. Furthermore, models or equations estimating operation velocity were also developed in many works [27–29]. In "Green Book" by AASHTO [8], contents related to scenic roads were stated. However, this statement is insufficient for practical works, and abovementioned studies merely concerned scenic roads whose design basis and indices were mainly directly adopted from those used in ordinary rural roads.

To study vertical alignment in scenic roads, the relationship between vertical grade and slope length should be specified. Typical vehicles travelling uphill with the specific weight-to-power ratio tend to lose operation velocity to some extent. The velocity reduction is restricted by some certain requirements, for instance, safety, affection on traffic flow, and traffic efficiency [8, 23, 30–33]. It is concluded from these studies that the dynamic model of the typical vehicle is a prerequisite of the vertical alignment design. In ordinary rural roads, heavy vehicles are always selected. However, as mentioned previously, electric or ethanol-consuming EFV is widely used in scenic roads, which reflects

different dynamic characters. Therefore, a model representing EFV dynamic characters is needed in this research.

Traditionally, the vehicle is simulated as a point mass in AASHTO Green Book [8], whose motion is examined independently in vertical and lateral directions. Following this classical model, compensations were made in several aspects, including the bicycle model used for simulating the vehicle by an axle in the steady state cornering [34], a transient formulation of the bicycle model used in cases of variable steering inputs [11], and the sophisticated multibody vehicle model (CarSim and TruckSim) used for high-reliability vehicle stability prediction in automotive industry [35–37]. According to related research studies, a multibody vehicle model considering the complex and real uphill travel environment will be developed in this research, which is used to assess the EFV motion problem.

3. Multibody Vehicle Model in Uphill

MLS and LSL are basically determined by dynamic characteristics of the vehicle when climbing a slope. When the vehicle starts to climb up at a specific initial velocity, it begins to decelerate due to the resistance brought by the slope. According to actual driving experience, the output driving force will increase at this moment if the output power remained unchanged. At a time point, the vehicle will reach a mechanical equilibrium condition, and it will be operated at a lower stable velocity. During the process described above, the vehicle will travel a specific length, on which MLS and LSL determined will largely depend. To study MLS and LSL based on dynamic performance of typical vehicles driven on roads in scenic spots, the static equilibrium state and dynamic balancing process should be studied as the basis of this paper.

3.1. Static Equilibrium State of the Typical Vehicle. As depicted in the previous part, the vehicle will operate at a relatively lower stable velocity in the static equilibrium state. The purpose of this part is to find out the stable velocity when climbing a slope with specific gradient and initial climbing velocity. The static force condition of a typical vehicle on a slope, according to classical mechanics theory, is shown in Figure 1. In this figure, M (kg) represents the total mass of the vehicle, $F(N)$ represents the driving force, $R_a(N)$ represents the air resistance, $R_r(N)$ represents the rolling resistance, $R_g(N)$ represents the slope resistance, and $\alpha(^\circ)$ stands for the elevation angle of the slope.

According to automotive dynamics theory and the analysis shown above, the effective driving force F_t and the maximum driving force $F_{\max}$ could be calculated by using the following equation:

$$F_t = 3600\left(\frac{P_e}{V}\right)\eta_T, \qquad F_{\max} = 9.8066 M_{ta}\mu. \tag{1}$$

In equation (1), P_e (kW) stands for engine power, V (km/h) stands for operation velocity, and η_T stands for transmission efficiency which can be found in reference [38];

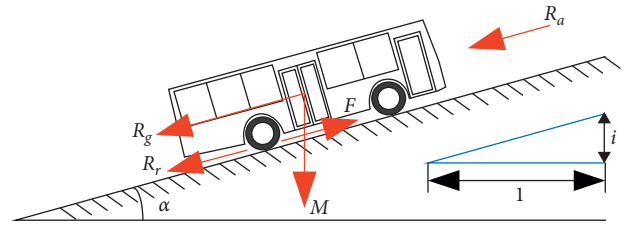

Figure 1: The static force condition of an EFV on a slope.

In equation (1), M_{ta} (kg) stands for total weight acting on the drive shaft and μ stands for the road friction coefficient, which can be found in reference [39].

As depicted in Figure 1, resistance forces R_a, R_r, and R_g should also be considered. Based on related aerodynamic research studies and experiments [39], the air resistance R_a could be calculated using the following equation:

$$R_a = \frac{C_d C_h}{21.15} A V^2, \qquad C_h = 1 - \xi H. \tag{2}$$

In equation (2), $A(\mathrm{m}^2)$ stands for the frontal area of the vehicle, C_d stands for the air resistance coefficient which is related to the vehicle type and can be found in reference [39], and the parameter C_h represents the altitude factor which could be calculated by altitude H (m), and in the plain area, $C_h = 1$. Taking rolling resistance R_r into consideration, the types of tire, road surface conditions, and operation velocity are deciding factors. It could be calculated by the following equation:

$$R_r = 9.8006 C_r (c_1 + c_2 V)\left(\frac{M}{1000}\right). \tag{3}$$

In equation (3), C_r refers to the rolling factor, which is related to road surface conditions and the parameters c_1 and c_2 refer to the rolling friction coefficient, which is related to the tire pattern. The values of the three parameters mentioned above could be found in reference [39]. According to classical mechanics theory, the slope resistance R_g could be obtained using the following equation:

$$R_g = 9.8006 M \sin\alpha = 9.8006 M i. \tag{4}$$

According to the static equilibrium state mentioned above, the driving force of the velocity equals to the joint force of resistance forces R_a, R_r, and R_g, and we have the following equation:

$$\begin{cases} P_e = F_i V_i = aV^3 + bV^2 + cV, \\ a = \dfrac{C_d C_h A}{77400\eta_T}, \\ b = \dfrac{C_r c_2 M}{367308\eta_T}, \\ c = \left(\dfrac{C_r c_1 M}{367308\eta_T}\right) + \left(\dfrac{Mi}{367.3\eta_T}\right). \end{cases} \tag{5}$$

From equation (5), when a typical vehicle is climbing a slope, the stable velocity under the static equilibrium state is

determined by output power P_e (which could be represented by initial velocity V_i and gradient i). However, the process of reaching this static equilibrium state could not be described using abovementioned analysis, and MLS and LSL are still unknown.

3.2. Dynamic Balancing Process of the Typical Vehicle. When a typical vehicle is climbing a slope with constant output power, LSL is defined as the travel distance of this vehicle when it reaches a static equilibrium state, as introduced in the previous part. In this dynamic process, the real-time acceleration $a(t_i)$ of the typical vehicle at time point t_i could be calculated using the following equation:

$$a(t_i) = \frac{(F(t_i) - R(t_i))}{M}. \tag{6}$$

The real-time motion state of the typical vehicle could be expressed in the following equation:

$$\begin{aligned} \frac{d[V(t_i)]}{dt} &= a(t_i), \\ \frac{d[X(t_i)]}{dt} &= V(t_i), \\ V(t_i) &= V(t_{i-1}) + a(t_{i-1})\Delta t, \\ X(t_i) &= X(t_{i-1}) + V(t_{i-1})\Delta t, \\ t_i - t_{i-1} &= \Delta t \cong 0. \end{aligned} \tag{7}$$

It is known that output power P_e is the product depending on driving force F_i and real-time velocity V_t. When P_e remains constant, it is necessary to discuss the initial driving force F_i and the initial velocity V_i because they will determine the motion state of the typical vehicle in this dynamic balancing process. At initial time point t_i, the typical vehicle begins to climb the slope with specific gradient i. Assuming $F_i > R_a + R_r + R_g$, due to the constant P_e, the travel velocity will increase, while the driving force will fall down. In the end of this dynamic process t_e, driving force F_e will be equal to the sum of R_a, R_r, and R_g, and the typical vehicle will stop its acceleration. The process of this condition is depicted using the blue line in Figure 2. In another circumstance $F_i < R_a + R_r + R_g$, it is easy to know that the travel velocity will decrease, while the driving force will rise and finally get to the static equilibrium state. The process of this condition is depicted using the red line in Figure 2.

4. Numerical Simulation of EFV Climbing Velocity

As depicted in Section 1, the dynamic performance of EFV in scenic spots differs from it of ordinary vehicles. Therefore, numerical simulation of EFV climbing velocity based on the multibody vehicle model is carried out, considering the typical EFV type obtained from field research. From Figure 2, the fundamental of determining LSL on a certain slope with specific initial velocity is provided. In practical

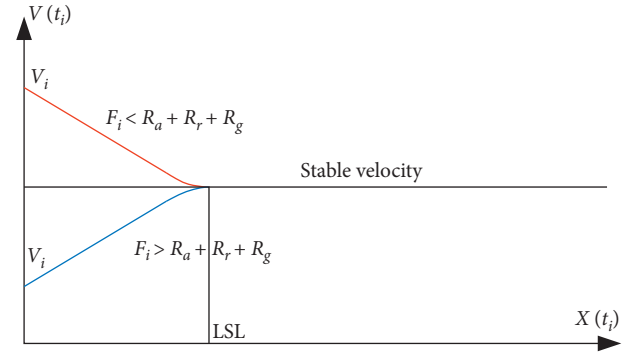

Figure 2: Schematic diagram of the dynamic motion process.

application, the phenomenon depicted by the blue line is rarely found because in most cases, the driver will maintain a relatively higher velocity in the flat area. If the situation expressed by the blue line happened, there is still no need to deal with it because it will not negatively affect the driver and traveler. Therefore, in this research, the situation of $F_i < R_a + R_r + R_g$ is analyzed.

However, the circumstance of the red line in Figure 2 could be interpreted as an extreme situation, which means the driver and the traveler will not show any dissatisfaction and intervention, and this is obviously unreasonable. In reality, large velocity loss in the slope section always causes serious safety risk. Therefore, the concept of maximum velocity loss (MVL) is defined in related road design criteria, which equals to 50% of designed velocity (DV) [39]. Furthermore, as the road in scenic spots, the satisfaction and comfort of the travelers should also be considered. For the most important reason, slope sections can be commonly seen in scenic roads. If MVL in slope sections is too large, it will further reduce the travelers' transmission efficiency and causes tourist backlog. Thus, another concept of ideal velocity loss (IVL) is defined based on above description and a lot of studies, including Cuihua Mountain National Park, Taiping Forest Park, and Huashan Mountain National Park. According to the results of field studies, the value of IVL is determined as 10 km/h.

The purpose of numerical simulation is to find the theoretical values of LSL in slopes with the specific gradient using the dynamic model provided in Section 3. The indices of MVL and IVL mentioned above were used as two principles to determine LSL. As depicted in Section 3, several parameters related to EFV should be chosen before calculation. According to the results of field studies, the parameters of the typical EFV type were obtained (Jinlong XMQ6801G type), with $M/P_e = 87$ kg/kW and $P_e = 132$ kW. Combining the operation velocity in abovementioned scenic roads, initial climbing velocity was chosen, as shown in Table 2, and 4%–11% was chosen as the slope gradient according to field research.

From Section 3, it is found that the stable velocity could be directly calculated using equation (5) after the parameters related to the vehicle are determined. However, the value of LSL could not be calculated using equation (7). To model the process of climbing a slope, iterative calculation was adopted in numerical simulation, and a simulation program was

Table 2: Initial climbing velocity in numerical simulation.

Initial climbing velocity (km/h)	60	50	40	30
MVL (km/h)	30	25	20	15
IVL (km/h)	10	10	10	10

developed based on Visual Basic. The framework of this program is shown in Figure 3, and it outputs the simulation results expressed by a two-dimensional image, the horizontal axis represents the length EFV traveled, and the vertical axis represents the operation velocity. The results of numerical simulation are shown in Figure 4.

Before analyzing the results given above, the method of defining LSL should be provided. As depicted in the previous part, MVL and IVL are principles of defining LSL. The parameter of IVL could be expressed as a loose boundary in Figure 4, shown as a red dotted line in the upper position of the figures. Under the condition of specific initial velocity (understood as operation velocity) and specific slope gradient, if the stable velocity remained larger than the value determined by IVL, then it could be described as the slope will not affect the travelers' experience; further, it will definitely satisfy the safety criteria MVL. The index of MVL could be seen as the restricted boundary of climbing a slope with specific gradient and initial velocity because the velocity drops too fast in this condition which affects the operation safety. In Figure 4, it is depicted as a red dotted line in the lower position of the figures. If the stable velocity exceeds this boundary, the slope will not satisfy the safety criteria in this condition, and not to mention the travelers' experience criteria IVL. The line in the top position (60 km/h-4%, 50 km/h-5%, 40 km/h-6%, and 30 km/h-6%) in each figure in Figure 4 does not reach the loose boundary in above-mentioned contents. According to the description, there is no need to determine the LSLs using these lines. Besides, the line in the bottom position (60 km/h-8%, 50 km/h-9%, 40 km/h-10%, and 30 km/h-11%) in each figure in Figure 4 exceeds the restricted boundary depicted in the previous part. It is known that these four conditions should not exist in the real scenic road design because they break the safety criteria. Apart from the eight lines mentioned above, the left are all situated between the boundaries based on MVL and IVL. Using IVL as the principle of determining LSL by considering the feeling of the travelers, the intersections of the curves and the upper boundaries are read as the theoretical values of LSLs (expressed as Theo. in the table), given in Table 3. Further, if the stable velocity of a specific slope equals to the lower boundary, then the maximum longitudinal slope (MLS) could be obtained using equation (5), as shown in Table 3. Besides, the LSLs used in previous road design criteria are provided as comparisons (expressed as Used in the table).

5. Model Verification

The data shown in Table 3 were obtained based on the theoretical model provided in Section 2. Though the detailed information of the vehicle and the road were considered in this model, the accuracy of the model still should be verified because the real climbing condition could not be completely and precisely simulated. Therefore, model verification is provided in this part based on the experiments in real scenic road sections.

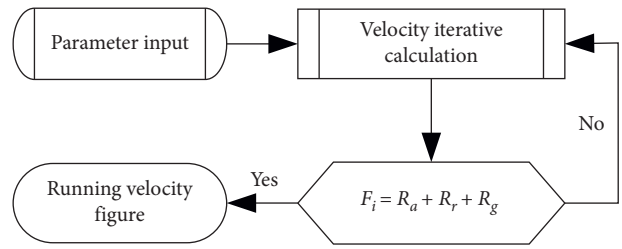

Figure 3: The framework of the simulation program.

5.1. The Field Experiments. As depicted in Section 3, the theoretical results were obtained based on the typical large-passenger EFV type Jinlong XMQ6801G, shown in Figure 5(a), and this vehicle type has a large market penetration rate in scenic spots. Therefore, the field experiments will be carried out using this vehicle type. In addition, to further validate the accuracy and the practicality of the model, the small passenger EFV type Wuling WLQ2110 ($M/P_e = 57$ kg/kW, $P_e = 28.5$ kW) used in Huashan Mountain was adopted in this field experiment, carrying water bags to increase load, seen in Figure 5(b). Besides, from the analysis in the previous part, some vehicle operation conditions could be concluded.

(i) A flat road section should be provided before climbing the slope, which will guarantee the EFV a stable initial velocity

(ii) The EFV should maintain a stable output power, and the driver should keep a specific gear position (third gear in this experiment) when climbing the slope

(iii) The EFV used in this experiment should be in the full-load status to keep the same condition used in numerical simulation

(iv) The slope should have an enough length to collect available and stable data

(v) The slope gradient could not be completely continuous and stable, but there should not be a large gradient change in a single chosen slope

Following these operation conditions, nine scenic road slope sections were chosen in three scenic spots, which were Huashan Mountain, Cuihua Mountain National Park, and Taiping Forest Park. The detailed information is provided in Table 4.

The OES noncontact photoelectric velocity sensor, including silicon photocell, optical system, and computer, was used to collect the climbing real-time velocity, as shown in Figure 5(c). The resolution for collecting running velocity, distance, time, and deceleration is 0.1 km/h, 1 mm, 1 ms, and 0.1 m/s^2, respectively. And, the accuracy of the four indicators above is 0.5%, 0.2%, 0.1%, and 1%, separately. The

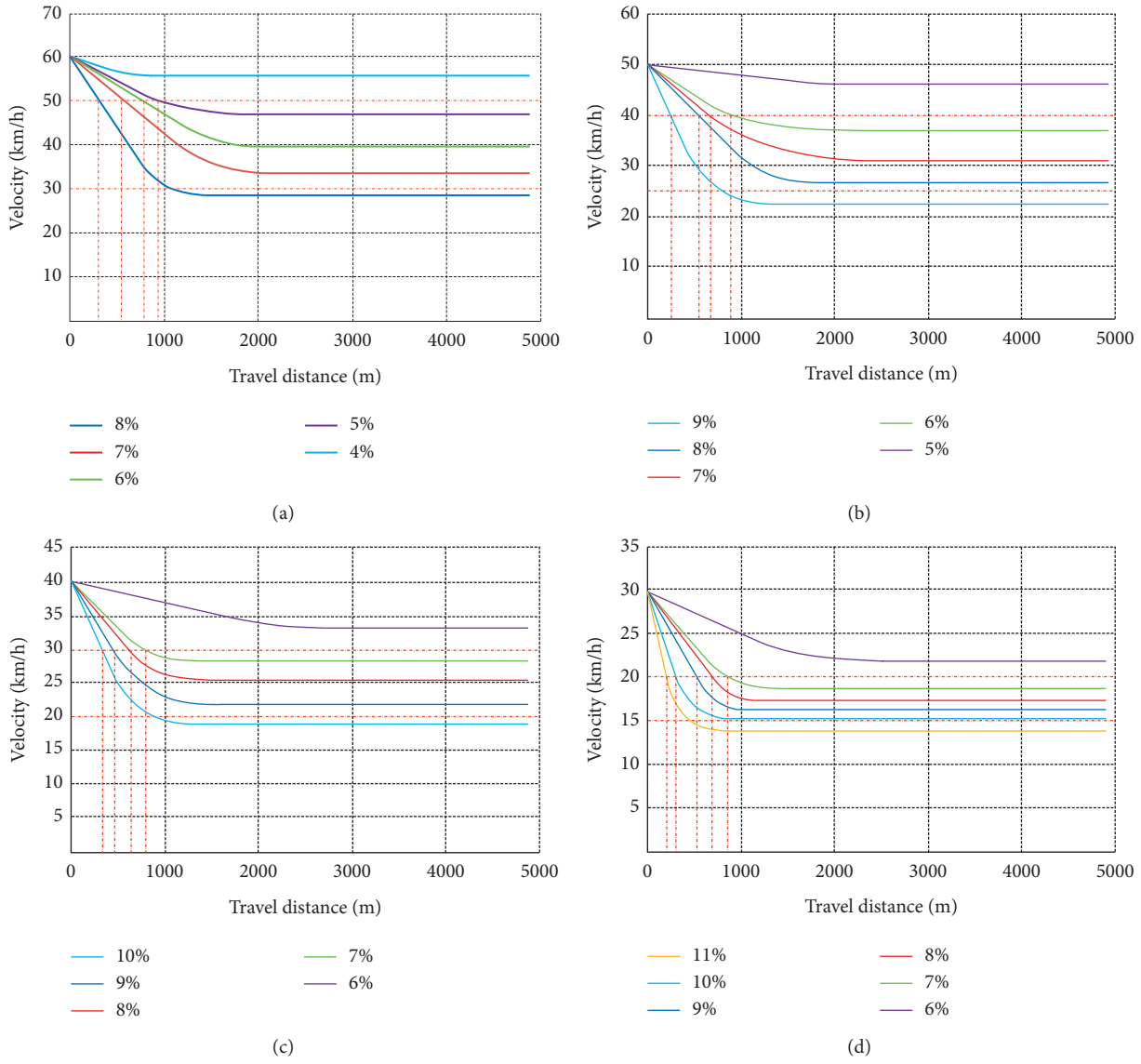

Figure 4: The results of numerical simulation. (a) Simulation results of initial velocity of 60 km/h. (b) Simulation results of initial velocity of 50 km/h. (c) Simulation results of initial velocity of 40 km/h. (d) Simulation results of initial velocity of 30 km/h.

Table 3: The theoretical values of LSLs.

Operation velocity (km/h)		60		50		40		30	
MLS (%)		7.8		8.4		9.7		10.2	
LSL (m)		Theo.	Used	Theo.	Used	Theo.	Used	Theo.	Used
Slope gradient (%)	5	955	800	—	—	—	900	—	900
	6	720	600	843	—	—	700	—	700
	7	512	—	639	—	825	500	960	500
	8	—	—	433	—	573	300	730	300
	9	—	—	—	—	427	—	505	200
	10	—	—	—	—	—	—	296	—
	11	—	—	—	—	—	—	—	—

drivers participating in this experiment are all EFV full-time drivers, and they were alcohol, coffee, and tea forbidden for 72 hours before the experiment. In the experiment, the driver was required to enter the specific slope with stable velocity shown in Table 3, following the second principle given above. Each climbing test was repeated for three times

Figure 5: Equipment used in this experiment. (a) Jinlong XMQ6801G. (b) Wuling WLQ2110. (c) Photoelectric velocity sensor.

Table 4: The detailed information of chosen slopes.

Number	Slope gradient (%)	Slope length (m)	Operation velocity (km/h)	Location	EFV type
1	8.6	105	40		
2	9.6	205	30	Huashan Mountain	Jinlong XMQ6801G
3	10.0	160	30		
4	6.5	210	60		
5	8.0	163	50	Taiping Forest Park	Jinlong XMQ6801G
6	7.5	165	50		
7	13.0	119	30		
8	14.8	145	30	Cuihua Mountain National Park	Wuling WLQ2110
9	16.0	120	30		

to obtain enough and reliable data, which comprised a single test group. In one climbing test, the real-time data were output meter by meter, and they were used to verify the theoretical model.

5.2. The Model Verification. As depicted in Section 4, field experiments were carried out in nine slope sections using two EFV types, and each climbing test was repeated for three times. To verify the mechanical model in Section 3, theoretical climbing velocities were calculated using the program in Section 4, and actual climbing velocities were obtained by averaging the values in three tests abovementioned. The results were shown in Figure 6. In these figures, the red straight lines stand for theoretical values, and the curved parts seen in Figure 4 were not depicted because the slope length was not long enough. Further, the blue polylines represent the actual velocities collected in the field experiment. Seen from these figures directly, actual velocities are distributed nearby the theoretical values, and their overall trends appeared the same. In Figures 6(a)–6(f), the accuracy of the mechanical model based on EFV Jinlong XMQ6801G was proved. In Figures 6(g)–6(i), the model using EFV Wuling WLQ2110 was also proved to be accurate. The relative errors between theoretical values and collected values were shown in Table 5.

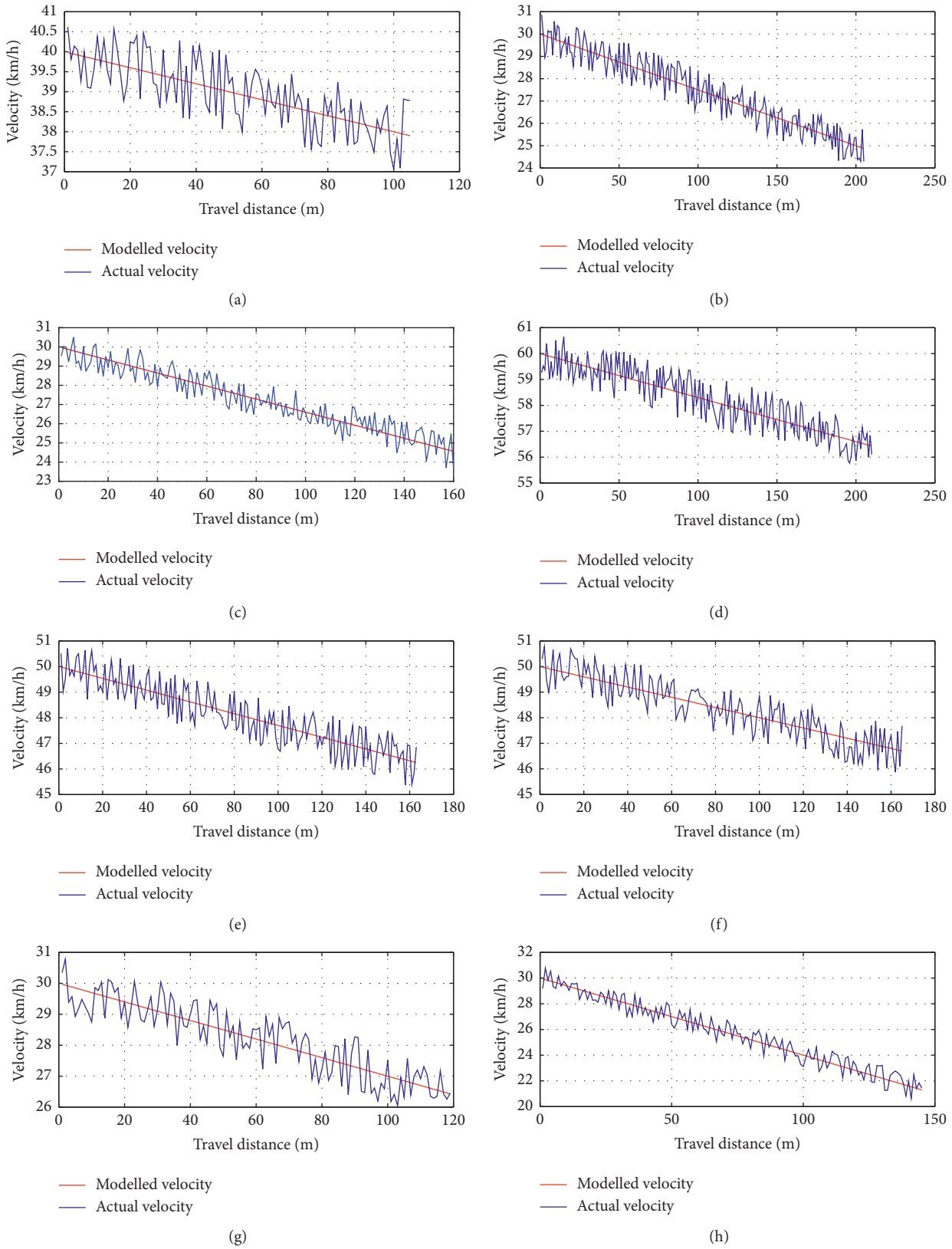

Figure 6: Continued.

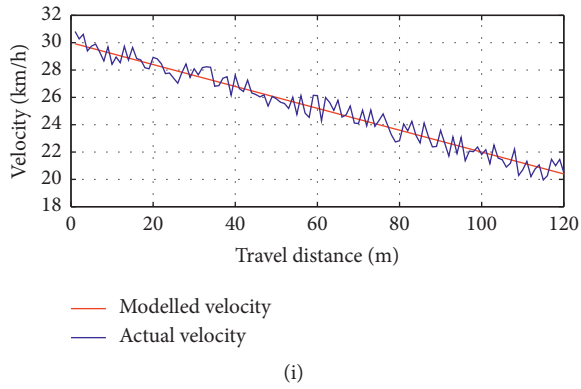

(i)

Figure 6: The results of model validation. (a) Slope 1. (b) Slope 2. (c) Slope 3. (d) Slope 4. (e) Slope 5. (f) Slope 6. (g) Slope 7. (h) Slope 8. (i) Slope 9.

Table 5: The relative errors between theoretical values and collected values.

Slope number	Relative errors	EFV type
1	0.0143	Jinlong XMQ6801G
2	0.0184	
3	0.0202	
4	0.0090	Jinlong XMQ6801G
5	0.0108	
6	0.0104	
7	0.0187	Wuling WLQ2110
8	0.0201	
9	0.0205	

6. Discussion

As shown in Figure 6, relative errors of the typical vehicle Jinlong XMQ6801G using the multibody vehicle model varied from 0.0090–0.0184, and relative errors of the typical vehicle Wuling WLQ2110 varied from 0.0187–0.0205. In summary, the vehicle dynamic model showed basically the same accuracy in simulating different typical vehicle's dynamic characters. With high accuracy of the dynamic model, curves obtained in Figure 4 could be directly used in practice under different principles. Here, it provides a comparison between curves in Figure 4 and related ones from AASHTO Green Book [8], as shown in Figure 7.

As shown in Figure 7, the curve results of AASHTO display the same trend compared to results in this article, which proves the practicality of the dynamic model. However, a large gap apparently exists. The typical vehicle adopted in AASHTO Green Book has the specific weight-to-power ratio of 120 kg/kW, but EFVs used in this study have the weight-to-power ratio of 87 kg/kW and 57 kg/kW. The longitudinal slope in this research varies from 4%–11%, and the longitudinal slope in Figure 7 varies from 0%–9%. Moreover, uphill travelling velocity loss in Figure 7 is much larger than that in Figure 4. Taking the instance of 9% grade as an example, velocity loss in Figure 7 is more than 80 km/h, but the largest velocity loss in Figure 4 is about 28 km/h, owing to special dynamic characters of EFV. Besides, situations depicted in AASHTO Green Book are somehow simpler, involving two initial velocities, 110 km/h and 70 km/h. Situations depicted in Figure 4 are more detailed, involving four initial velocities, 60 km/h, 50 km/h, 40 km/h, and 30 km/h. In conclusion, the results in this article are more practical in the domestic scenic road design.

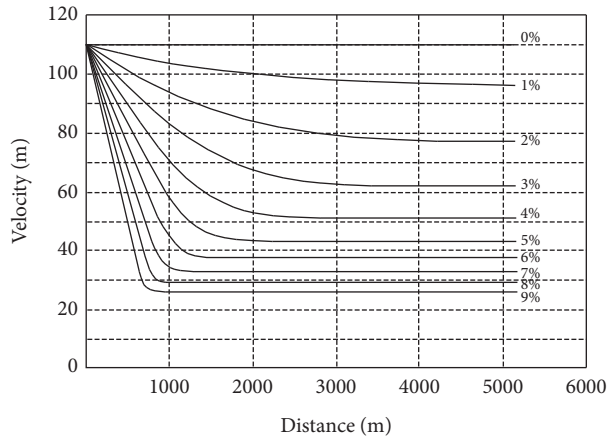

Figure 7: Velocity variation curves of uphill travelling under different longitudinal gradients in AASHTO Green Book [8].

In Table 3, MLSs and LSLs obtained using the dynamic model are compared with those in current criteria, as shown in Table 1. When operation velocities are 60 km/h, 40 km/h, and 30 km/h, MLSs used in current criteria are 6%, 7%, and 8%, respectively, and MLSs obtained in Table 3 are 7.8%, 9.7%, and 10.2%, respectively, obviously larger than current criteria values. Besides, operation velocity of 50 km/h is not provided in current criteria. Considering the values of LSLs in Table 3 and Table 1, it could be seen that, values in this article are larger than those in current criteria. This could be also contributed to the superior characters of modern EFV. Integrating the large gap and scenic road environment, data in Table 3 are practical.

7. Conclusions

In this research, MLS and LSL values applicable to scenic roads using EFV are provided. The multibody vehicle model

in uphill was established, providing the static equilibrium state and dynamic balancing process of the typical vehicle. Based on this model, MLS and LSL values in scenic roads were obtained using numerical simulation, considering typical EFV, MVL representing travel safety, and IVL representing travel efficiency. MLS values in scenic roads using EFV obtained in this research vary from 7.8%–10.2%, which are larger than current criteria values. LSL values obtained vary from 200–955 m, which are also larger than current criteria values. To prove the accuracy of the dynamic model, also the practicality of MLS and LSL values, field experiments were carried out in Huashan Mountain, Cuihua Mountain National Park, and Taiping Forest Park, using two EFV types. According to the verification results, the relative errors of climbing velocity vary from 0.0104–0.0205, showing the dynamic model's accuracy.

Almost all of scenic spots are under the sealed management, and private passenger vehicles are forbidden to run in the scenic spots in China. Roads' alignment design in the scenic spots must consider the characteristics of the vehicles running in the scenic spots and environment protection. There was little guideline for MLS and LSL values applicable to scenic roads using EFV. The results could make up this shortage. Furthermore, the MLS and LSL values used for EFV are larger than current criteria values (6%–8% of MLS and 200 = 900 m of LSL) used for the typical vehicles running on the highways or freeways. The total length of the scenic roads can be shortened, and the cut and fill volumes can be decreased, which will be beneficial for the natural landscape through making the route alignment fitting the terrain much better and reducing damage to the environment. The planners and designers can use the MLS and LSL values to design the vertical alignment of the roads in scenic spots.

This research can lay a foundation for establishing the vertical alignment design for the roads in scenic spots. In the future, the technical indices and values of horizontal alignments should be studied through simulation and field experiments applicable for EFV. Furthermore, the coordination design of horizontal and vertical alignment should be proposed in order to perfect the geometric design for the roads in scenic spots.

Data Availability

The data used to support the findings of this study are available from the corresponding author upon request.

Conflicts of Interest

The authors declare that there are no conflicts of interest regarding the publication of this paper.

Acknowledgments

This research was funded by the National Key R&D Program of China (Grant nos. 2018YFB1600302 and 2018YFB1600300) and partly supported by the Science Foundation Project of Chongqing Jiaotong University (Grant no. 20JDKJC-B001).

References

[1] L. W. Green, *Yosemite: The Park and its Resources: Historical Resource Study*, National Park Service, Washington, DC, USA, 1987.

[2] H. H. Hochmair, *Towards a Classification of Route Selection Criteria for Route Planning Tools*, pp. 481–492, Springer, Berlin, Germany, 2004.

[3] S. F. Witt and C. A. Witt, "Forecasting tourism demand: a review of empirical research," *International Journal of Forecasting*, vol. 11, no. 3, pp. 447–475, 1995.

[4] F. C. Jaarsma and F. Van Langevelde, "The motor vehicle and the environment: balancing between accessibility and habitat fragmentation," in *Proceedings of the 29th ISATA, Dedicated Conference on the Motor Vehicle and the Environment*, pp. 299–306, Florence, Italy, February 1996.

[5] W.-C. Hong, "Traffic flow forecasting by seasonal SVR with chaotic simulated annealing algorithm," *Neurocomputing*, vol. 74, no. 12-13, pp. 2096–2107, 2011.

[6] T. Williams, "The unkindest cuts," *Audubon*, vol. 100, no. 1, pp. 24–31, 1998.

[7] F. C. Jaarsma, "Rural low-traffic roads (LTRs): the challenge for improvement of traffic safety for all road users," in *Proceedings of the 27th ISATA, Dedicated Conference on Road and Vehicle Safety*, Aachen, Germany, November 1994.

[8] American Association of State Highway and Transportation Officials, *A Policy on Geometric Design of Highway and Streets*, AASHTO, Washington, DC, USA, 2018.

[9] J. M. Dargay and M. B. F. Hanly, *Elasticities. Interim Report to the Department of the Environment Transport and the Regions*, ESRC Transport Studies Unit, London, UK, 1999.

[10] CCCC First Highway Consultants Co., Ltd., *Design Specification for Highway alignment*, China Communications Publishing & Media Management Co., Ltd., Beijing, China, 2017.

[11] H. B. Pacejka, *Tire and Vehicle Dynamics*, Society of Automotive Engineers. Inc., London, UK, 2006.

[12] J. Zhang, H. Kawasaki, and Y. Kawai, "A tourist route search system based on web information and the visibility of scenic sights," in *Proceedings of the IEEE 2008 Second International Symposium on Universal Communication*, pp. 154–161, Osaka, Japan, December 2008.

[13] R. E. Manning, *Studies in Outdoor Recreation: Search and Research for Satisfaction*, Oregon State University Press, Corvallis, OR, USA, 2nd edition, 1999.

[14] R. E. Manning, *Parks and Carrying Capacity: Commons without Tragedy*, Island Press, Washington, DC, USA, 2007.

[15] C. F. Jaarsma, "Approaches for the planning of rural road networks according to sustainable land use planning," *Landscape and Urban Planning*, vol. 39, no. 1, pp. 47–54, 1997.

[16] T. Tang, Y. Guo, X. Zhou, S. Labi, and S. Zhu, "Understanding electric bike riders' intention to violate traffic rules and accident proneness in China," *Travel Behaviour and Society*, vol. 23, pp. 25–38, 2021.

[17] D. N. Cole and P. B. Landres, "Threats to wilderness ecosystems: impacts and research needs," *Ecological Applications*, vol. 6, no. 1, pp. 168–184, 1996.

[18] Countryside Commission, *Visitors to National Parks Summary of the 1994 Survey Findings: Technical Report*, Countryside Commission, Cheltenham, UK, 1996.

[19] Yorkshire Dales National Park, *The 1994 National Parks Visitor Survey, Key Findings*, Yorkshire Dales National Park, Bainbridge, UK, 1996.

[20] T. J. Steiner and A. L. Bristow, "Road pricing in national parks: a case study in the Yorkshire Dales National Park," *Transport Policy*, vol. 7, no. 2, pp. 93–103, 2000.

[21] P. B. Goodwin, "A review of new demand elasticities with special reference to short and long run effects of price change," *Journal of Transport Economics and Policy*, vol. 26, no. 2, pp. 155–169, 1992.

[22] Transportation Research Board, *Highway Capacity Manual*, TRB, Washington, DC, USA, 5th edition, 2010.

[23] CCCC First Highway Consultants Co., Ltd., *Technical Standard of Highway Engineering*, China Communications Publishing & Media Management Co., Ltd., Beijing, China, 2014.

[24] G. Kanellaidis and S. Vardaki, "Highway geometric design from the perspective of recent safety developments," *Journal of Transportation Engineering*, vol. 137, no. 12, pp. 841–844, 2011.

[25] S. Jung, K. Wang, C. Oh, and J. Chang, "Development of highway safety policies by discriminating freeway curve alignment features," *KSCE Journal of Civil Engineering*, vol. 22, no. 4, pp. 1418–1426, 2018.

[26] D. B. Fambro, K. Fitzpatrick, and C. W. Russell, "Operating speed on crest vertical curves with limited stopping sight distance," *Transportation Research Record: Journal of the Transportation Research Board*, vol. 1701, no. 1, pp. 25–31, 2000.

[27] D. R. Jessen, K. S. Schurr, P. T. McCoy, G. Pesti, and R. R. Huff, "Operating speed prediction on crest vertical curves of rural two-lane highways in Nebraska," *Transportation Research Record: Journal of the Transportation Research Board*, vol. 1751, no. 1, pp. 67–75, 2001.

[28] H. Gong and N. Stamatiadis, "Operating speed prediction models for horizontal curves on rural four-lane highways," *Transportation Research Record: Journal of the Transportation Research Board*, vol. 2075, no. 1, pp. 1–7, 2008.

[29] J. Tang, F. Liu, W. Zhang, R. Ke, and Y. Zou, "Lane-changes prediction based on adaptive fuzzy neural network," *Expert Systems with Applications*, vol. 91, pp. 452–463, 2018.

[30] R. Archilla and J. Morrall, "Traffic characteristics on two-lane highway downgrades," *Transportation Research Part A: Policy and Practice*, vol. 30, no. 2, pp. 119–133, 1996.

[31] C. M. Morris and E. T. Donnell, "Passenger car and truck operating speed models on multilane highways with combinations of horizontal curves and steep grades," *Journal of Transportation Engineering*, vol. 140, no. 11, 2014.

[32] L. Wang, J.-C. Cheng, and Y.-L. Zhang, "Reliability-based specification on critical length of highway sections with near-maximum grade," *KSCE Journal of Civil Engineering*, vol. 22, no. 4, pp. 1406–1417, 2018.

[33] Y. Guo, Y. Li, P. C. Anastasopoulos, S. Peeta, and J. Lu, "China's millennial car travelers' mode shift responses under congestion pricing and reward policies: a case study in Beijing," *Travel Behaviour and Society*, vol. 23, pp. 86–99, 2021.

[34] M. Kontaratos, B. Psarianos, and A. Yiotis, "Minimum horizontal curve radius as a function of grade incurred by vehicle motion in driving mode," *Transportation Research Record: Journal of the Transportation Research Board*, vol. 1445, no. 1, pp. 86–93, 1994.

[35] T.-H. Chang, "Effect of vehicles' suspension on highway horizontal curve design," *Journal of Transportation Engineering*, vol. 127, no. 1, pp. 89–91, 2001.

[36] S. Mavromatis and B. Psarianos, "Analytical model to determine the influence of horizontal alignment of two-axle heavy vehicles on upgrades," *Journal of Transportation Engineering*, vol. 129, no. 6, pp. 583–589, 2003.

[37] T. Varunjikar, *Design of Horizontal Curves with Downgrades Using Loworder Vehicle Dynamics Models*, Master of Science Thesis, The Pennsylvania State University, University Park, PA, USA, 2011.

[38] T. Watanada, *The Highway Design and Maintenance Standard Model, V.1: Description of the HDM-III Model*, The Johns Hopkins University Press, Baltimore, MA, USA, 1987.

[39] J. W. Fitch, *Motor Truck Engineering Handbook*, Society of Automotive Engineers, Warrendale, PA, USA, 1993.